

HATS-13b and HATS-14b: two transiting hot Jupiters from the HATSouth survey^{*}

L. Mancini¹, J. D. Hartman², K. Penev², G.Á. Bakos², R. Brahm^{3,4}, S. Ciceri¹, Th. Henning¹, Z. Csubry², D. Bayliss⁵, G. Zhou⁶, M. Rabus^{3,1}, M. de Val-Borro², N. Espinoza^{3,4}, A. Jordán^{3,4}, V. Suc³, W. Bhatti², B. Schmidt⁶, B. Sato⁷, T. G. Tan⁸, D. J. Wright², C. G. Tinney², B. C. Addison⁹, R. W. Noyes¹⁰, J. Lázár¹¹, I. Papp¹¹, and P. Sári¹¹

¹ Max Planck Institute for Astronomy, Königstuhl 17, 69117 – Heidelberg, Germany
e-mail: mancini@mpa.de

² Department of Astrophysical Sciences, Princeton University, Princeton, NJ 08544, USA

³ Instituto de Astrofísica, Pontificia Universidad Católica de Chile, Av. Vicuña Mackenna 4860, 7820436 Macul, Santiago, Chile

⁴ Millennium Institute of Astrophysics, Av. Vicuña Mackenna 4860, 7820436 Macul, Santiago, Chile

⁵ Observatoire Astronomique de l'Université de Genève, 51 ch. des Maillettes, 1290 Versoix, Switzerland

⁶ The Australian National University, Canberra, Australia

⁷ Department of Earth and Planetary Sciences, Tokyo Institute of Technology, 2-12-1 Ookayama, Meguro-ku, Tokyo 152-8551, Japan

⁸ Perth Exoplanet Survey Telescope, Perth, Australia

⁹ Exoplanetary Science Group, School of Physics, University of New South Wales, Sydney, NSW 2052, Australia

¹⁰ Harvard-Smithsonian Center for Astrophysics, Cambridge, MA 02138 USA

¹¹ Hungarian Astronomical Association, Budapest, Hungary

Preprint online version: July 26, 2018

ABSTRACT

We report the discovery of HATS-13b and HATS-14b, two hot-Jupiter transiting planets discovered by the HATSouth survey. The host stars are quite similar to each other (*HATS-13*: $V = 13.9$ mag, $M_\star = 0.96 M_\odot$, $R_\star = 0.89 R_\odot$, $T_{\text{eff}} \approx 5500$ K, $[\text{Fe}/\text{H}] = 0.05$; *HATS-14*: $V = 13.8$ mag, $M_\star = 0.97 M_\odot$, $R_\star = 0.93 R_\odot$, $T_{\text{eff}} \approx 5350$ K, $[\text{Fe}/\text{H}] = 0.33$) and both the planets orbit around them with a period of ~ 3 days and a separation of ~ 0.04 au. However, even though they are irradiated in a similar way, the physical characteristics of the two planets are very different. HATS-13b, with a mass of $M_p = 0.543 \pm 0.072 M_J$ and a radius of $R_p = 1.212 \pm 0.035 R_J$, appears as an inflated planet, while HATS-14b, having a mass of $M_p = 1.071 \pm 0.070 M_J$ and a radius of $R_p = 1.039 \pm 0.032 R_J$, is only slightly larger in radius than Jupiter.

Key words. stars: planetary systems – stars: fundamental parameters – stars: individual: HATS-13 (aka GSC 6928-00497) – stars: individual: HATS-14 (aka GSC 6926-00259) – techniques: radial velocities – techniques: photometric

1. Introduction

After 20 years from when the human knowledge crossed the borders of the solar system and found a planet orbiting another main sequence star (Mayor & Queloz 1995), we can now count more than 1800 exoplanets in our Galaxy,

^{*} The HATSouth network is operated by a collaboration consisting of Princeton University (PU), the Max Planck Institute für Astronomie (MPIA), the Australian National University (ANU), and the Pontificia Universidad Católica de Chile (PUC). The station at Las Campanas Observatory (LCO) of the Carnegie Institute is operated by PU in conjunction with PUC, the station at the High Energy Spectroscopic Survey (H.E.S.S.) site is operated in conjunction with MPIA, and the station at Siding Spring Observatory (SSO) is operated jointly with ANU. Based in part on observations made with (i) the Subaru Telescope, which is operated by the National Astronomical Observatory of Japan; (ii) the MPG 2.2m and the (iii) Euler 1.2m Telescopes at the ESO Observatory in La Silla; (iv) the CTIO 0.9m Telescope at the Observatory of Cerro Tololo.

and marvel how physically varied and intriguing most of them are. The first class of *unexpected* planets with which we faced is composed by the so-called *hot Jupiters*, i.e. giant gaseous planets in close orbits around their host stars, able to perform a complete orbit in a relatively short time ($\sim 0.1 - 10$ days). Even though they are rarer than small-size rocky and Neptunian planets (Fressin et al. 2013; Dressing & Charbonneau 2013; Petigura et al. 2013), there are numerous reasons that make them very interesting to study, especially those that transit their parent stars. Indeed, since hot Jupiters are more massive and larger than rocky planets, it is possible to measure their physical parameters with a much better accuracy: *in primis* mass and radius, but also their spin-orbit alignment (from the Rossiter-McLaughlin effect), their thermal flux and reflected light (from *occultations* and *phase curve*), the chemical composition of their atmosphere (from *emission* and *transmission spectra*), etc. However, although all these parameters are accessible, even with moderate-sized ground-based telescopes, there are various aspects

of the hot-Jupiter population that were not well understood. We did not find, for example, any convincing way to group them in classes based on some of their features (e.g., Hansen & Barman 2007; Fortney et al. 2008; Schlaufman 2010; Madhusudhan 2012). It is also very puzzling to determine what are the physical mechanisms that regulate the formation, accretion, evolution and cause the migration of giant planets from the snow line (~ 3 au) up to roughly 0.01 au from their host stars. In this context, several scaling laws have been suggested between their parameters (e.g., Southworth et al. 2007; Knutson et al. 2010; Hartman 2010), but none seems to be generally apply to all planets.

Answering the above questions is possible only by enlarging the sample at our disposal, in particular the regions of the parameter space which are currently deserted because of observational biases. In the last three *lustra*, ground-based transit surveys have played a major role in exoplanet detection and thus in the growth of our scientific knowledge about planetary systems. In a fair competition with other teams (e.g., HATNet: Bakos et al. 2004; WASP: Pollacco et al. 2006; KELT: Pepper et al. 2007; MEARTH: Charbonneau et al. 2009; QES: Alsubai et al. 2013; APACHE: Sozzetti et al. 2013; NGTS: Wheatley et al. 2013), we are undertaking the HATSouth project, which consists of the monitoring of millions of stars in the southern sky to look for new exoplanet transit signals. Our survey is carried out by a network of 6 telescope systems, employing 24 astrographs, distributed over three continents (South America, Africa, and Australia), thus increasing the sensitive to long-period (> 10 days) planets (Bakos et al. 2013).

Here we present two new transiting extrasolar planets: HATS-13b and HATS-14b. The paper is organized as follows: in Sect. 2 we summarize the detection of the photometric transit signal and the subsequent spectroscopic and photometric observations of each star to confirm the planets. In Sect. 3 we analyze the data to rule out false positive scenarios, and to determine the stellar and planetary parameters. Our findings are summarized and discussed in Sect. 4.

2. Observations

2.1. Photometric detection

The *modus operandi* of the HATSouth survey is comprehensively described in Bakos et al. (2013). In brief, HATSouth is a network of completely automated wide-field telescopes, consisting in six homogeneous units located at three different places in the southern hemisphere, i.e. Las Campanas Observatory (LCO) in Chile, the H.E.S.S. site in Namibia, and Siding Spring Observatory (SSO) in Australia. Each unit is equipped with four 18 cm $f/2.8$ Takahasi astrographs, each working in pairs with Apogee U16M Alta 4k \times 4k CCD cameras, with a total mosaic field-of-view on the sky of $8^\circ \times 8^\circ$ at a scale of 3.7 arcsec pixel $^{-1}$. Observations are performed through a Sloan- r filter with an exposure time of 4 minutes. Scientific images are automatically calibrated and light curves are extracted by aperture photometry. They are then treated with decorrelation and detrending algorithms¹ and finally run through with

BLS (Box-fitting Least Squares; Kovács et al. 2002) to find periodic signals by transiting exoplanets.

The stars HATS-13 (aka 2MASS 21075075-2605479; $\alpha = 21^h07^m50.88s$, $\delta = -26^\circ05'48.0''$; J2000) and HATS-14 (aka 2MASS 20525171-2541144; $\alpha = 20^h52^m51.60s$, $\delta = -25^\circ41'14.4''$; J2000) are two moderately bright ($V = 13.89$ mag and $V = 13.79$ mag, respectively) stars. They were monitored between Nov 2009 and September 2010 by three of the HATSouth units, which collected more than 10 000 images for both of them. Details of the observations are reported in Table 1. The corresponding light curves, folded with a period of $P \sim 3.04$ and 2.77 days, respectively, are plotted in Fig. 1, both clearly showing transiting-planet signals with depths of $\sim 2\%$ and $\sim 1\%$, respectively.

2.2. Spectroscopic Observations

After being selected as *HATSouth* planet candidates, HATS-13 and HATS-14 underwent spectral reconnaissance through low- and medium-resolution observations with the Wide Field Spectrograph (WiFeS; Dopita et al. 2007) mounted on the ANU 2.3 m telescope at SSO. This first step is very useful in the planet confirmation process because it can immediately rule out possible false positive cases, mainly caused by giant stars, F-M binary systems and blending with faint eclipsing-binary systems.

Using WiFeS, we identified both the targets as dwarf stars. HATS-13 and HATS-14 were then accurately monitored with an array of telescopes equipped with high-resolution spectrographs, covering wide ranges of optical wavelengths, to look for possible radial-velocity (RV) variations compatible with the presence of planetary companions.

Four and five spectra were observed in May 2012 for HATS-13 and HATS-14, respectively, with CYCLOPS mounted on the 3.9 m Anglo-Australian Telescope at SSO. A better RV accuracy was achieved between May and November 2012 thanks to FEROS (Kaufer & Pasquini 1998) on the MPG 2.2 m telescope at the ESO Observatory in La Silla and Coralie (Queloz et al. 2001) on the Euler 1.2 m telescope, also located in La Silla. In total, with these two instruments, we collected 32 and 31 spectra for HATS-13 and HATS-14, respectively, with an average precision of some tens of meters per second. Information about these spectroscopic observations are summarized in Table 2, yet we did not use all the spectra in the analysis, as some of them were discarded due to high-sky contamination. Additional details about the instruments and data-reduction processes are exhaustively discussed in previous works of the HATS team and we refer the reader to those (i.e. Penev et al. 2013; Mohler-Fischer et al. 2013; Bayliss et al. 2013). In particular, Coralie and FEROS spectra were reduced using the new procedure described in Jordán et al. (2014) and Brahm et al. (2015).

To better characterize the periodic signal of the RV variation of HATS-13, it was necessary to observe this target with higher RV precision. On September 2012, we used the High Dispersion Spectrograph (HDS; Noguchi et al. 2002) on the Subaru telescope at the Observatory of Mauna Kea, Hawaii. Observations were spread over four nights and performed in a way similar to those for HATS-5 (Zhou et al. 2014), i.e. using a $0''.6 \times 2''.0$ slit and a setup which guaranteed a wavelength-range coverage of 3500 – 6200 Å, with

¹ External Parameter Decorrelation (EPD; Bakos et al. 2010); Trend Filtering Algorithm (TFA; Kovács et al. 2005).

Table 1. Summary of photometric observations

Instrument/Field ^a	UT Date(s)	# Images	Cadence ^b (sec)	Filter	Precision ^c (mmag)
HATS-13					
HS-2/G582	2009 Nov–2010 Sep	2486	288	<i>r</i>	12.6
HS-4/G582	2009 Sep–2010 Sep	8565	288	<i>r</i>	12.2
HS-6/G582	2010 Apr–2010 Sep	356	265	<i>r</i>	13.1
CTIO 0.9m ^d	2012 Aug 26	68	237	<i>z</i>	2.9
GROND ^d	2012 Oct 17	82	87	<i>g</i>	1.4
GROND ^d	2012 Oct 17	83	87	<i>r</i>	1.2
GROND ^d	2012 Oct 17	82	87	<i>i</i>	1.7
GROND ^d	2012 Oct 17	82	87	<i>z</i>	1.6
PEST	2013 May 3	99	130	<i>R</i>	4.7
PEST	2013 Jun 30	189	130	<i>R</i>	4.7
HATS-14					
HS-2/G582	2009 Nov–2010 Sep	4866	284	<i>r</i>	11.5
HS-4/G582	2009 Sep–2010 Sep	8889	288	<i>r</i>	12.6
HS-6/G582	2010 Aug–2010 Sep	200	290	<i>r</i>	11.6
PEST	2013 Jun 06	131	131	<i>R</i>	4.8
GROND ^d	2013 Jun 12	114	192	<i>g</i>	1.6
GROND ^d	2013 Jun 12	114	192	<i>r</i>	1.8
GROND ^d	2013 Jun 12	114	192	<i>i</i>	2.6
GROND ^d	2013 Jun 12	114	192	<i>z</i>	2.0

Notes.

^a For HATSouth data we list the HATSouth unit and field name from which the observations are taken. HS-1 and -2 are located at Las Campanas Observatory in Chile, HS-3 and -4 are located at the H.E.S.S. site in Namibia, and HS-5 and -6 are located at Siding Spring Observatory in Australia. Each field corresponds to one of 838 fixed pointings used to cover the full 4π celestial sphere. All data from a given HATSouth field are reduced together, while detrending through External Parameter Decorrelation (EPD) is done independently for each unique field+unit combination.

^b The median time between consecutive images rounded to the nearest second. Due to weather, the day–night cycle, guiding and focus corrections, and other factors, the cadence is only approximately uniform over short timescales.

^c The RMS of the residuals from the best-fit model.

^d The *telescope-defocussing* technique (Southworth et al. 2009) was used for this transit observation.

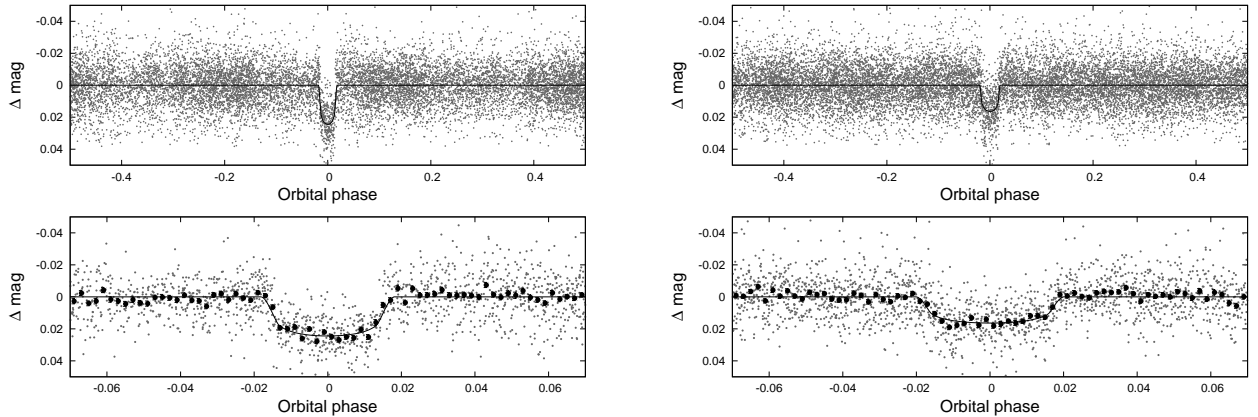


Fig. 1. Phase-folded unbinned HATSouth light curves for HATS-13 (*left*) and HATS-14 (*right*). In each case we show two panels. The top panel shows the full light curve, while the bottom panel shows the light curve zoomed-in on the transit. The solid lines show the model fits to the light curves. The dark filled circles in the bottom panels show the light curves binned in phase with a bin size of 0.002.

a resolution of $R = 60\,000$. Ten spectra were taken using an I_2 cell and another three without it (Table 2). All of HDS observations were reduced following Sato et al. (2002, 2012).

All the RV measurements, extracted from the spectra here discussed, are listed in Table A.2 and A.3. Phased RV and BS measurements are shown for each system in Fig. 2.

2.3. Photometric follow-up observations

High-quality photometric follow-up observations of additional transit events of the two targets were subsequently performed with larger telescopes than the HATSouth units. This is also an important step because it allowed us to have a precise light-curve anatomy of the planetary transits (depth, duration and sharpness) and – by constraining the eccentricity via RV variations – measure the mean density of the parent stars with high accuracy and with no

Table 2. Summary of spectroscopy observations

Telescope/Instrument	UT Date(s)	# Spec.	Res. $\Delta\lambda/\lambda/1000$	S/N Range ^a	$\gamma_{\text{RV}}^{\text{b}}$ (km s ⁻¹)	RV Precision ^c (m s ⁻¹)
HATS-13						
ANU 2.3 m/WiFeS	2012 Apr 10	1	3	90
ANU 2.3 m/WiFeS	2012 Apr 11-12	2	7	30-40	25.0	1000
AAT 3.9 m/CYCLOPS	2012 May 5-11	4	70	10-20	25.8	190
Euler 1.2 m/Coralie	2012 Jun-Nov	9	60	12-17	25.8	100
MPG 2.2 m/FEROS	2012 May-Oct	23	48	29-72	25.8	68
Subaru 8 m/HDS	2012 Sep 19	3	60	17-32
Subaru 8 m/HDS+I ₂	2012 Sep 20-22	10	60	15-27	...	21
HATS-14						
ANU 2.3 m/WiFeS	2012 Apr 10	1	3	70
ANU 2.3 m/WiFeS	2012 Apr 11-13	3	7	23-31	28.5	380
AAT 3.9 m/CYCLOPS	2012 May 5-11	5	70	15-25	29.9	110
Euler 1.2 m/Coralie	2012 Jun-Nov	14	60	9-16	30.2	37
MPG 2.2 m/FEROS	2012 May-2013 Jul	17	48	25-68	30.2	12

Notes.^a S/N per resolution element near 5180 Å.^b For Coralie, FEROS and CYCLOPS this is the systemic RV from fitting an orbit to the observations in 3.3. For WiFeS it is the mean of the observations, and for the du Pont Echelle it is the measured RV of the single observation. We do not provide this quantity for instruments for which only relative RVs are measured, or for the lower resolution WiFeS observations which were only used to measure stellar atmospheric parameters.^c For High-precision RV observations included in the orbit determination this is the RV residuals from the best-fit orbit, for other instruments used for reconnaissance spectroscopy this is an estimate of the precision, or the measured standard deviation.

systematic errors (Seager & Mallén-Ornelas 2003). As we will see in Sect. 3.1 the knowledge of the stellar mean density is a very useful constraint for the determination of the other physical parameters of the two systems.

Concerning HATS-13, two complete and two incomplete transits were observed using the MPG 2.2 m, the CTIO 0.9 m, and the PEST 0.3 m telescopes. Two complete transit events were successfully monitored for HATS-14 with the MPG 2.2 m and PEST telescopes. Relevant information about these observations (i.e. dates, cadence, filter, precision) are reported in Table 1. In particular, the MPG 2.2 m telescope is equipped with GROND, a multi-imaging camera, able to observe a field-of-view (FOV) of $5.4' \times 5.4'$ in four different filters (similar to Sloan g, r, i, z) simultaneously (Greiner et al. 2008). Details of the GROND camera and data reduction are reported in Penev et al. (2013) and Mohler-Fischer et al. (2013), while studies of the accuracy and S/N expectations for this instrument were done by Pierini et al. (2012) and Mancini et al. (2014). The PEST telescope and data reduction method are discussed in Bayliss et al. (2013). The same information for the CTIO 0.9 m telescope have been reported by Hartman et al. (2014).

The light curves for HATS-13 and HATS-14 are shown in Fig. 3 and Fig. 4, respectively. The corresponding data, including those from the HATS units, are given in Table 3.

3. Analysis

Based on the data previously presented, this section is dedicated to the derivation of the physical parameters of the HATS-13 and HATS-14 planet hosts.

3.1. Properties of the parent stars

We used 17 and 14 high-resolution FEROS spectra to determine the *atmospheric* properties (metallicity, effective

temperature and surface gravity) of the stars HATS-13 and HATS-14, respectively. This was accomplished by using the new routine ZASPE (Zonal Atmospheric Stellar Parameter Estimator), which is fully described in Brahm et al. (2015). The other principal stellar parameters (like mass, radius, luminosity, age, etc.) and corresponding uncertainties were estimated thanks to a Markov chain Monte Carlo (MCMC) global analysis of our photometric and spectroscopic data, following the methodology of Sozzetti et al. (2007). This is based on stellar effective temperature $T_{\text{eff}\star}$, which we determined with ZASPE, the stellar mean density ρ_{\star} , estimated from the light-curve fitting (see Sect. 3.3), and from the Yonsei-Yale (YY; Yi et al. 2001) evolutionary tracks.

Spanning a range of reliable values for the metallicity, we calculated the YY isochrones for each of the two systems over a wide range of ages and compared the resulting $T_{\text{eff}\star}$ and ρ_{\star} with those estimated from the data. The best agreement returned the values of the other stellar parameters. In particular, the better estimation of the stellar logarithmic surface gravity ($\log g_{\star} = 4.524 \pm 0.017$ for HATS-13 and $\log g_{\star} = 4.484 \pm 0.020$ for HATS-14), was used for a second iteration of ZASPE, by fixing these values, to revise the other atmospheric parameters.

The stellar properties that we derived are reported in Table 3, along with their 1σ uncertainties. Model isochrones are shown in the panels of Fig. 5, in which the positions of the two stars in the $T_{\text{eff}\star} - \rho_{\star}$ diagram are also marked.

We found that both the stars are slightly smaller and less massive than the Sun, with parameters listed in Table 3. In particular, with $T_{\text{eff}\star} = 5523 \pm 69$ K, $M_{\star} = 0.962 \pm 0.029 M_{\odot}$, $R_{\star} = 0.887 \pm 0.019 R_{\odot}$, $B - V = 0.80 \pm 0.03$, $V - H = 1.84 \pm 0.04$, HATS-13 is a G5 V star, whereas HATS-14, characterized by $T_{\text{eff}\star} = 5346 \pm 60$ K, $M_{\star} = 0.967 \pm 0.024 M_{\odot}$, $R_{\star} = 0.933^{+0.023}_{-0.015} R_{\odot}$, $B - V = 0.83 \pm 0.2$, $V - H = 1.87 \pm 0.3$, has a spectral class close to the K/G transition (Pecaut & Mamajek 2013). The preferred

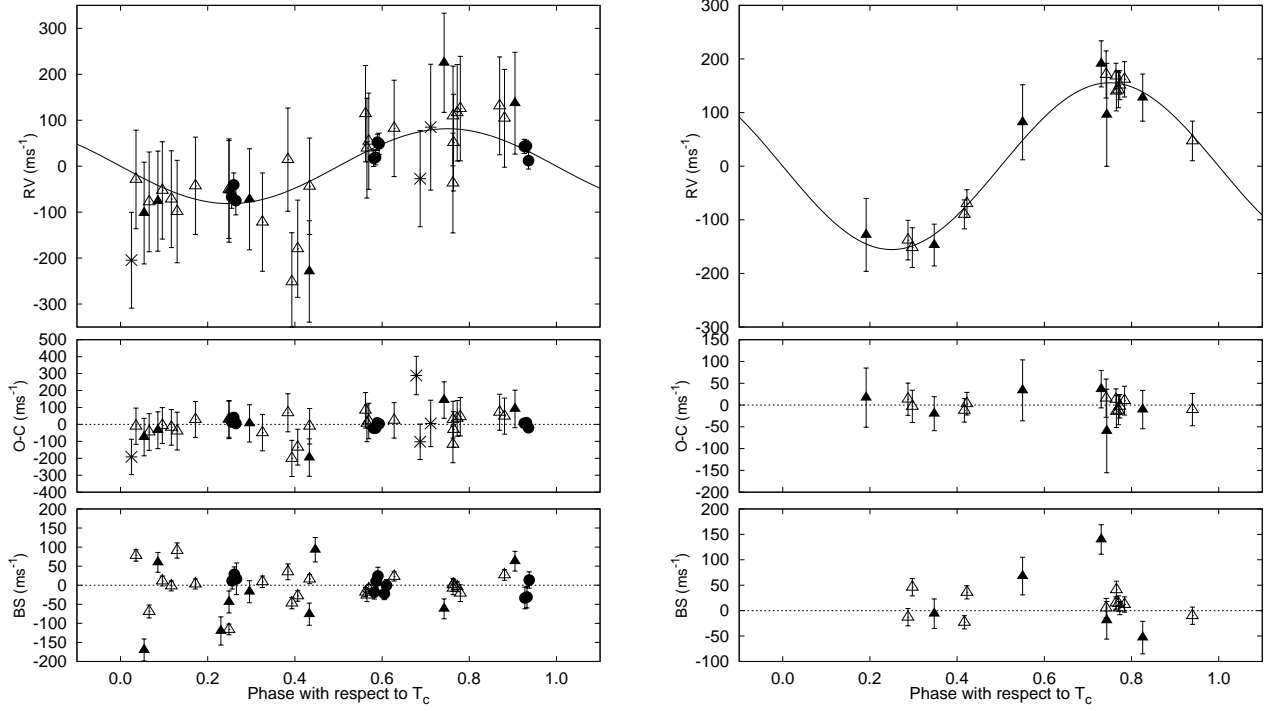


Fig. 2. Phased high-precision RV measurements for HATS-13 (*left*), and HATS-14 (*right*) from HDS (filled circles), FEROS (open triangles), Coralie (filled triangles), and CYCLOPS (stars). In each case we show three panels. The top panel shows the phased measurements together with our best-fit model (see Table 4) for each system. Zero-phase corresponds to the time of mid-transit. The center-of-mass velocity has been subtracted. The second panel shows the velocity O-C residuals from the best fit. The error bars include the jitter terms listed in Table 4 added in quadrature to the formal errors for each instrument. The third panel shows the bisector spans (BS), with the mean value subtracted. Note the different vertical scales of the panels.

metallicities are $[\text{Fe}/\text{H}] = 0.050 \pm 0.060$ and $[\text{Fe}/\text{H}] = 0.330 \pm 0.060$ for HATS-13 and HATS-14, respectively.

Table 3 also shows the magnitudes of the two stars in the optical bands (taken from APASS as listed in the UCAC 4 catalog; Zacharias et al. 2012) and in the NIR bands (from 2MASS). We compared these values with the predicted magnitudes in each filter from the isochrones, determining the distance of the two stars, that is 476 ± 12 pc for HATS-13 and 513 ± 14 pc for HATS-14. Here the extinction was estimated by assuming an $R_V = 3.1$ law from Cardelli et al. (1989).

3.2. Excluding blend scenarios

To rule out the possibility that either HATS-13 or HATS-14 is a blend between an eclipsing binary and a third star (potentially in the foreground or background of the binary), we carried out a blend analysis following Hartman et al. (2012). We find that for both objects the single star with a transiting planet model fits the light curves and broadband photometric color data better than a blended eclipsing binary model. For HATS-13 the best-fit transiting planet model is preferred with 2σ confidence over the best-fit blend model, while for HATS-14 the best-fit transiting planet model is preferred with 4σ confidence. Moreover, we find that any blend model that comes close to fitting the photometric data would have been easily detected as a composite object based on the spectroscopic data (there would be two clear peaks in the CCFs, the RVs from the highest peak would vary by more than 1 km s^{-1} , as would

the bisector spans). We conclude that both HATS-13 and HATS-14 are transiting planet systems. We cannot, however, rule out the possibility that either object is a blend between a transiting planet system and a third star that is fainter than the planet-hosting star. For HATS-13 we find that including a physical stellar companion with a mass greater than $0.84 M_\odot$ leads to a worse fit than not including the companion, however even a companion up to the mass of the primary star cannot be ruled out with greater than 5σ confidence. For HATS-14 we can rule out companions with a mass greater than $0.92 M_\odot$ with greater than 5σ confidence, while including a companion with a mass greater than $0.5 M_\odot$ leads to a worse fit of the data than a non-composite system. High-resolution imaging and/or long-term RV monitoring are needed to determine if either system has a stellar companion. For the remainder of the paper we assume both objects are single stars with transiting planets, however if either system has a stellar companion the true radius and mass of the planet would be larger than what we infer here.

3.3. Global modelling of the data

We modeled the HATSouth photometry, the follow-up photometry, and the high-precision RV measurements following Pál et al. (2008), Bakos et al. (2010), Hartman et al. (2012). We fit Mandel & Agol (2002) transit models to the light curves, allowing for a dilution of the HATSouth transit depth as a result of blending from neighboring stars and over-correction by the trend-filtering method. For the

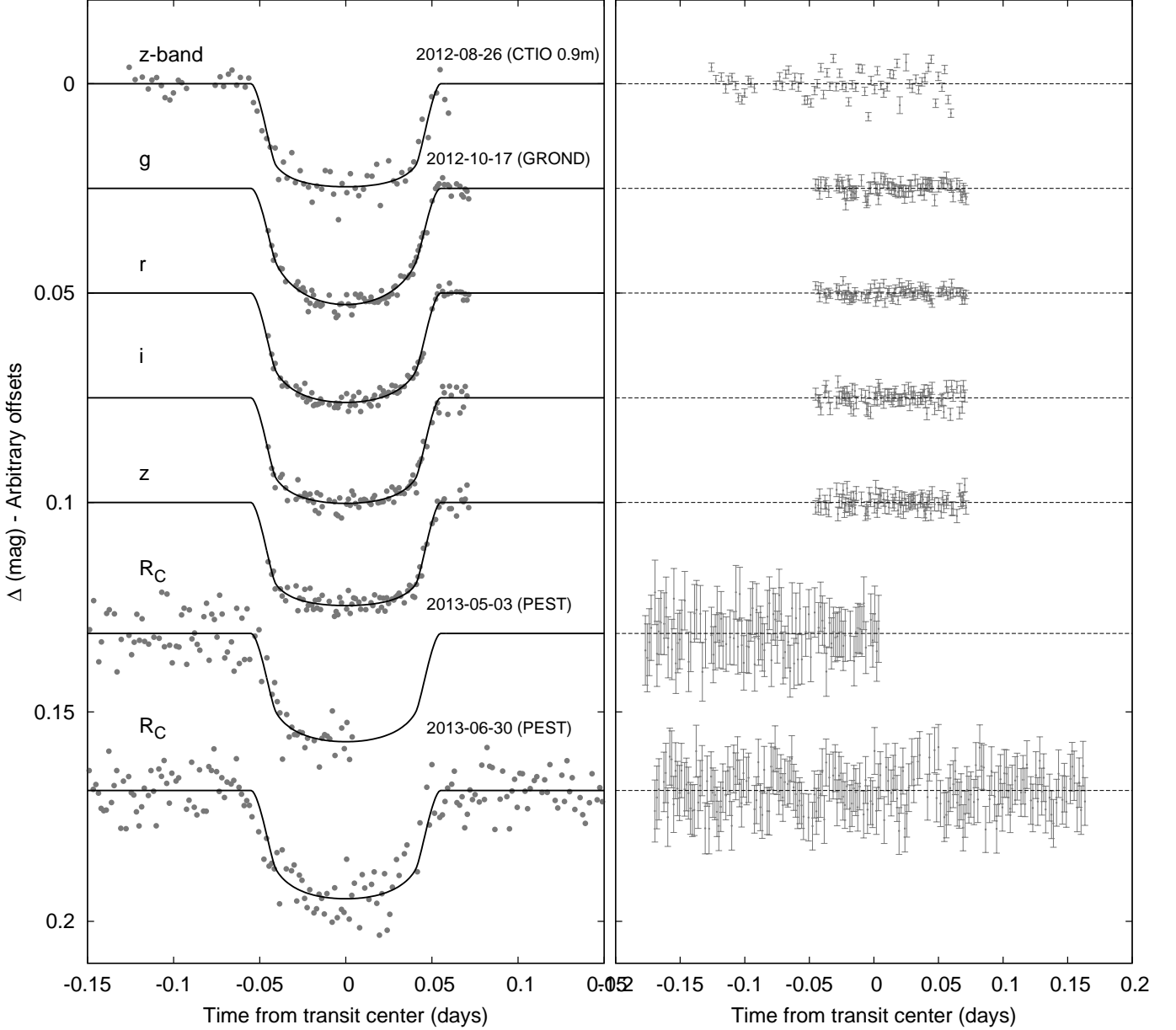


Fig. 3. *Left panel:* Unbinned transit light curves for HATS-13. The light curves have been corrected for quadratic trends in time fitted simultaneously with the transit model. The dates of the events, filters and instruments used are indicated. Light curves following the first are displaced vertically for clarity. Our best fit from the global modeling described in Sect. 3.3 is shown by the solid lines. *Right panel:* residuals from the fits are displayed in the same order as the left curves. The error bars represent the photon and background shot noise, plus the readout noise.

follow-up light curves we include a quadratic trend in time in our model for each event to correct for systematic errors in the photometry. We fit Keplerian orbits to the RV curves allowing the zero-point for each instrument to vary independently in the fit, and allowing for RV jitter which we also vary as a free parameter for each instrument. We used a Differential Evolution Markov Chain Monte Carlo procedure to explore the fitness landscape and to determine the posterior distribution of the parameters. One may see that for HATS-14 the scatter in the Coralie and FEROS RV residuals is consistent with the uncertainties (see Fig. 2), so our modelling finds jitter values of 0 for both instruments.

The resulting parameters for each system are listed in Table 4. They were determined assuming circular orbits.

We have also explored non-zero eccentricities, by varying $\sqrt{e} \cos \omega$ and $\sqrt{e} \sin \omega$ in the fitting process, e being the eccentricity and ω the argument of the periastron. In this case, we got that $e < 0.181$ (< 0.142) at 95% confidence for HATS-3 (HATS-4).

By inspecting Table 4, we can note that while HATS-14b has mass ($M_p = 1.071 \pm 0.070 M_J$) and size ($R_p = 1.039^{+0.032}_{-0.022} R_J$) slightly larger than those of Jupiter, HATS-13 is much less massive (only $M_p = 0.543 \pm 0.072 M_J$), but bloated ($R_p = 1.212 \pm 0.035 R_J$). The above values lead to mean densities extremely different, i.e. $\rho_p = 0.377 \pm 0.058 \text{ g cm}^{-3}$ for HATS-13b and $\rho_p = 1.191^{+0.098}_{-0.140} \text{ g cm}^{-3}$ for HATS-14b. Curiously, even though they have different phy-

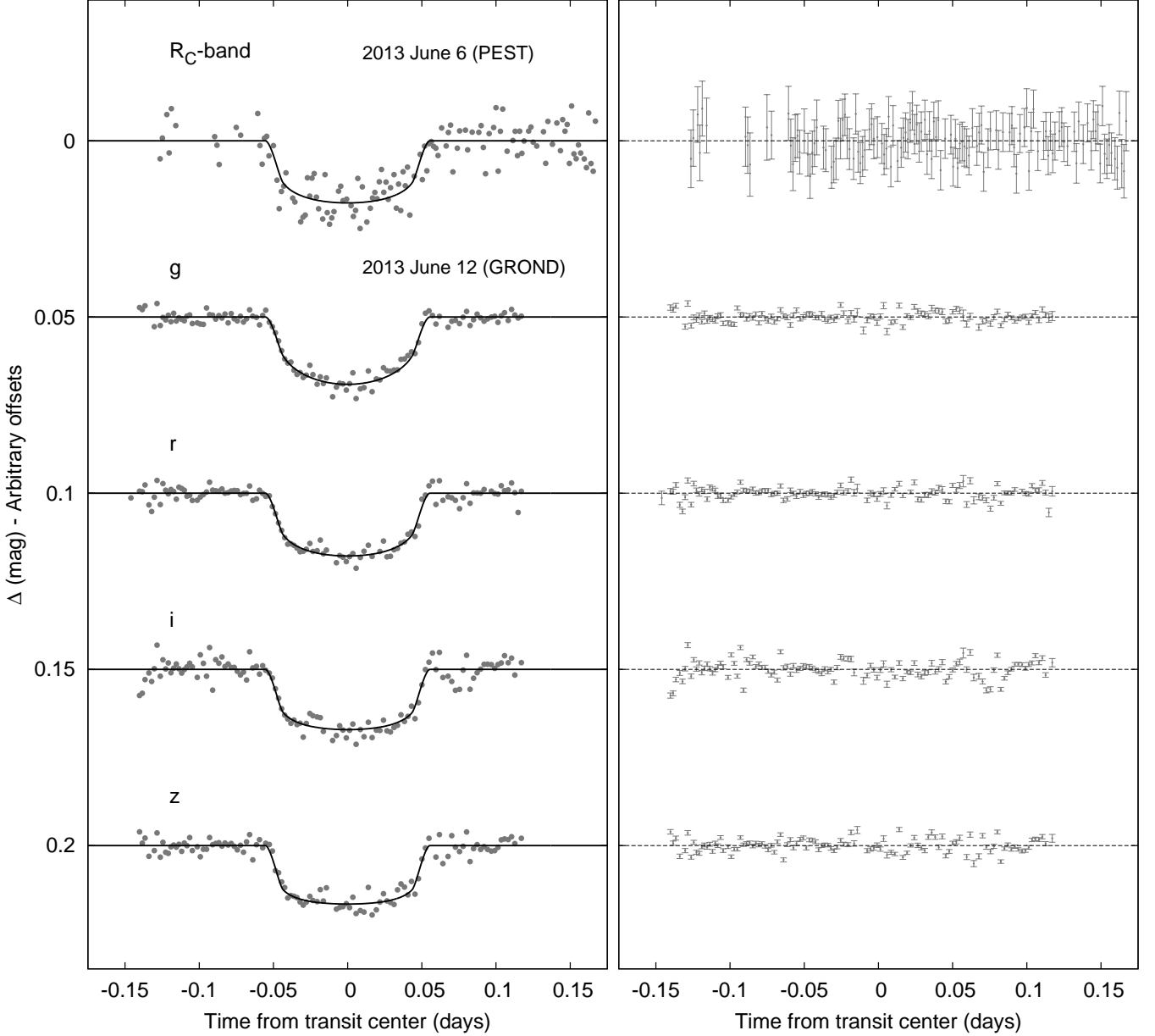


Fig. 4. Similar to Fig. 3; here we show the follow-up light curves for HATS-14.

sical properties, their orbital periods (3.04 and 2.77 days) and separation from the own host star (0.041 and 0.038 au) are similar to each other.

4. Discussion and conclusions

After having monitored more than 3 million stars in its almost first five years of life, the HATSouth survey is now entering in a phase of continuous flow of exoplanet discoveries. In this work we have presented two new hot-Jupiter transiting planets, HATS-13b and HATS-14b, both orbiting around slightly metal rich, mild main-sequence stars with a period of ~ 3 days. Their detection is robustly based on extensive photometric observations and numerous RV measurements, as we described in the previous sections.

Orbiting around similar stars at similar distances, the stellar radiation that the two planets receive are quite similar, i.e. ~ 5.4 and $\sim 6.0 \times 10^8 \text{ erg s}^{-1} \text{ cm}^{-2}$ for HATS-

13b and HATS-14b, respectively, putting them in the pL class, according to the terminology of Fortney et al. (2008). Based on their equilibrium temperature and surface gravity (see Table 4), their scale heights are ~ 740 and ~ 230 km, respectively. So, HATS-13b would be a suitable target for transmission-spectroscopy follow-up observations, but, since it is a pL planet, we do not expect that its atmosphere hosts a large amount of absorbing molecules in the optical wavelength range (Fortney et al. 2010). However, past observations of transiting gas giants reveal a wide diversity (e.g., Wakeford & Sing 2015) and a more sophisticated classification scheme for hydrogen-dominated exoplanetary atmospheres would be necessary (see Madhusudhan et al. 2014 and references therein).

If we look to their Safronov number, HATS-13b and HATS-14b would belong to separate classes of planets and should have had quite different evolution, migration and evaporation processes (Hansen & Barman 2007). Actually,

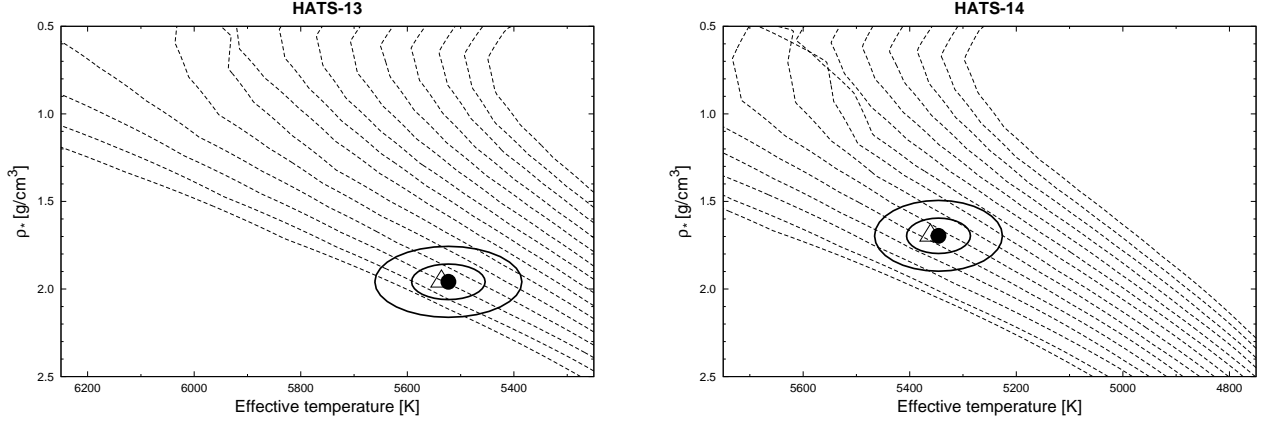


Fig. 5. Model isochrones from Yi et al. (2001) for the measured metallicities of HATS-13 (*left panel*) and HATS-14 (*right panel*). In each case we show models for ages of 0.2 Gyr and 1.0 to 14.0 Gyr increments (ages increasing from left to right). The adopted values of $T_{\text{eff}\star}$ and ρ_{\star} are shown together with their 1σ and 2σ confidence ellipsoids. The initial values of $T_{\text{eff}\star}$ and ρ_{\star} from the first ZASPE and light curve analyses are represented with a triangle.

Table 3. Stellar parameters for HATS-13 and HATS-14

Parameter	HATS-13b Value	HATS-14b Value	Source
Astrometric properties and cross-identifications			
2MASS-ID.....	2MASS 21075075-2605479	2MASS 20525171-2541144	
GSC-ID.....	GSC 6928-00497	GSC 6926-00259	
R.A. (J2000).....	21 ^h 07 ^m 50.88s	20 ^h 52 ^m 51.60s	2MASS
Dec. (J2000).....	−26°05′48.0″	−25°41′14.4″	2MASS
$\mu_{\text{R.A.}}$ (mas yr ^{−1})	−2 ± 14	0.4 ± 1.5	UCAC4
$\mu_{\text{Dec.}}$ (mas yr ^{−1})	−9.1 ± 1.6	−8.8 ± 1.3	UCAC4
Spectroscopic properties			
$T_{\text{eff}\star}$ (K).....	5523 ± 69	5346 ± 60	ZASPE ^a
[Fe/H].....	0.050 ± 0.060	0.330 ± 0.060	ZASPE
$v \sin i_{\star}$ (km s ^{−1})	2.82 ± 0.30	3.8 ± 1.2	ZASPE
γ_{RV} (km s ^{−1})	25.804 ± 0.014	30.190 ± 0.008	Coralie, FEROS
Photometric properties			
B (mag).....	14.686 ± 0.020	14.62 ± 0.10	APASS ^b
V (mag).....	13.887 ± 0.010	13.79 ± 0.10	APASS ^b
g (mag).....	14.217 ± 0.010	...	APASS ^b
r (mag).....	13.612 ± 0.010	...	APASS ^b
i (mag).....	13.392 ± 0.010	...	APASS ^b
J (mag).....	12.439 ± 0.021	12.518 ± 0.026	2MASS
H (mag).....	12.052 ± 0.025	12.129 ± 0.023	2MASS
K_s (mag).....	11.983 ± 0.028	12.037 ± 0.019	2MASS
Derived properties			
M_{\star} (M_{\odot}).....	0.962 ± 0.029	0.967 ± 0.024	YY+ ρ_{\star} +ZASPE ^c
R_{\star} (R_{\odot}).....	0.887 ± 0.019	0.933 ^{+0.023} _{−0.015}	YY+ ρ_{\star} +ZASPE
$\log g_{\star}$ (cgs).....	4.524 ± 0.017	4.484 ± 0.020	YY+ ρ_{\star} +ZASPE
ρ_{\star} (g cm ^{−3}).....	1.93 ± 0.11	1.682 ^{+0.071} _{−0.126}	YY+ ρ_{\star} +ZASPE ^d
L_{\star} (L_{\odot}).....	0.650 ± 0.051	0.640 ± 0.047	YY+ ρ_{\star} +ZASPE
M_V (mag).....	5.349 ± 0.096	5.399 ± 0.091	YY+ ρ_{\star} +ZASPE
M_K (mag,ESO).....	3.610 ± 0.054	3.525 ± 0.053	YY+ ρ_{\star} +ZASPE
Age (Gyr).....	2.5 ± 1.7	4.9 ± 1.7	YY+ ρ_{\star} +ZASPE
A_V (mag).....	0.152 ± 0.062	0.000 ± 0.033	YY+ ρ_{\star} +ZASPE
Distance (pc).....	476 ± 12	513 ± 14	YY+ ρ_{\star} +ZASPE

Notes.

^a ZASPE = Zonal Atmospheric Stellar Parameter Estimator routine for the analysis of high-resolution spectra (Brahm et al. 2015), applied to the FEROS spectra of HATS-13 and HATS-14. These parameters rely primarily on ZASPE, but have a small dependence also on the iterative analysis incorporating the isochrone search and global modeling of the data.

^b From APASS DR6 for HATS-13, HATS-14 as listed in the UCAC 4 catalog (Zacharias et al. 2012).

^c YY+ ρ_{\star} +ZASPE = Based on the YY isochrones (Yi et al. 2001), ρ_{\star} as a luminosity indicator, and the ZASPE results.

^d The parameter ρ_{\star} is primarily determined from the global fit to the light curves and RV data. The value shown here also has a slight dependence on the stellar models and ZASPE parameters due to restricting the posterior distribution to combinations of [ρ_{\star} , $T_{\text{eff}\star}$, Fe/H] that match to a YY stellar model.

Table 4. Orbital and planetary parameters for HATS-13b and HATS-14b

Parameter	HATS-13b Value	HATS-14b Value
Light curve parameters		
P (days)	3.0440499 ± 0.0000027	2.7667641 ± 0.0000027
T_c (BJD) ^a	$2456340.31705 \pm 0.00026$	$2456408.76462 \pm 0.00021$
T_{14} (days) ^a	0.10978 ± 0.00084	0.11009 ± 0.00078
$T_{12} = T_{34}$ (days) ^a	0.01430 ± 0.00063	0.01168 ± 0.00061
a/R_*	9.82 ± 0.18	$8.80^{+0.12}_{-0.22}$
ζ/R_* ^b	20.939 ± 0.090	20.35 ± 0.12
R_p/R_*	0.1402 ± 0.0016	0.1145 ± 0.0012
b^2	$0.062^{+0.035}_{-0.030}$	$0.032^{+0.058}_{-0.026}$
$b \equiv a \cos i/R_*$	$0.249^{+0.062}_{-0.071}$	$0.18^{+0.12}_{-0.10}$
i (deg)	88.55 ± 0.43	88.83 ± 0.66
Limb-darkening coefficients ^c		
c_1, g (linear term)	0.6213	0.7052
c_2, g (quadratic term)	0.1844	0.1193
c_1, r	0.4107	0.4725
c_2, r	0.2928	0.2569
c_1, i	0.3116	0.3562
c_2, i	0.3063	0.2871
c_1, z	0.2436	0.2739
c_2, z	0.3108	0.3035
c_1, R	0.3833	0.4404
c_2, R	0.2974	0.2661
RV parameters		
K (m s ⁻¹)	78 ± 10	158 ± 10
e ^d	< 0.181	< 0.142
RV jitter HDS (m s ⁻¹) ^e	0.0 ± 4.0	...
RV jitter FEROS (m s ⁻¹)	62 ± 14	0.00 ± 0.61
RV jitter Coralie (m s ⁻¹)	108 ± 41	0.0 ± 1.7
RV jitter CYCLOPS (m s ⁻¹) .	220 ± 130	...
Planetary parameters		
M_p (M_J)	0.543 ± 0.072	1.071 ± 0.070
R_p (R_J)	1.212 ± 0.035	$1.039^{+0.032}_{-0.022}$
C (M_p, R_p) ^f	0.07	-0.08
ρ_p (g cm ⁻³)	0.377 ± 0.058	$1.191^{+0.098}_{-0.140}$
$\log g_p$ (cgs)	2.961 ± 0.063	$3.394^{+0.026}_{-0.046}$
a (AU)	0.04057 ± 0.00041	0.03815 ± 0.00032
T_{eq} (K)	1244 ± 20	1276 ± 20
Θ ^g	0.0377 ± 0.0050	0.0814 ± 0.0058
$\log_{14} \langle F \rangle$ (cgs) ^h	8.732 ± 0.028	8.778 ± 0.027

Notes.

^a Times are in Barycentric Julian Date calculated directly from UTC *without* correction for leap seconds. T_c : Reference epoch of mid transit that minimizes the correlation with the orbital period. T_{14} : total transit duration, time between first to last contact; $T_{12} = T_{34}$: ingress/egress time, time between first and second, or third and fourth contact.

^b Reciprocal of the half duration of the transit used as a jump parameter in our MCMC analysis in place of a/R_* . It is related to a/R_* by the expression $\zeta/R_* = a/R_*(2\pi(1 + e \sin \omega))/(P\sqrt{1 - b^2}\sqrt{1 - e^2})$ (Bakos et al. 2010).

^c Values for a quadratic law, adopted from the tabulations by Claret (2004) according to the spectroscopic (ZASPE) parameters listed in Table 3.

^d As discussed in Sect. 3.3 the adopted parameters for all four systems are determined assuming circular orbits. We also list the 95% confidence upper limit on the eccentricity determined when $\sqrt{e} \cos \omega$ and $\sqrt{e} \sin \omega$ are allowed to vary in the fit.

^e Term added in quadrature to the formal RV uncertainties for each instrument. This is treated as a free parameter in the fitting routine.

^f Correlation coefficient between the planetary mass M_p and radius R_p estimated from the posterior parameter distribution.

^g The Safronov number is given by $\Theta = \frac{1}{2}(V_{\text{esc}}/V_{\text{orb}})^2 = (a/R_p)(M_p/M_*)$ (see Hansen & Barman 2007).

^h Incoming flux per unit surface area, averaged over the orbit.

even though the parent stars have similar masses, their inferred ages differ by a factor of ~ 2 (see Table 3). Fig. 6 shows the positions of the two new HATS planets in the current planet mass-radius plot (left panel) and planet mass-density plot (right panel). They are shown together with those of all the other known transiting exoplanets (data

taken from the TEPcat catalogue² on March 9, 2015). It can be noted immediately that they occupy two quite different positions in both the diagrams. In the left panel, HATS-14b appears to be a bit out from the population of Jupiters with masses near $1 M_J$, whereas HATS-13b is in the middle of a cluster of planets with masses around

² The Transiting Extrasolar Planet Catalogue (TEPcat) is available at www.astro.keele.ac.uk/jkt/tepcat/ (Southworth 2011).

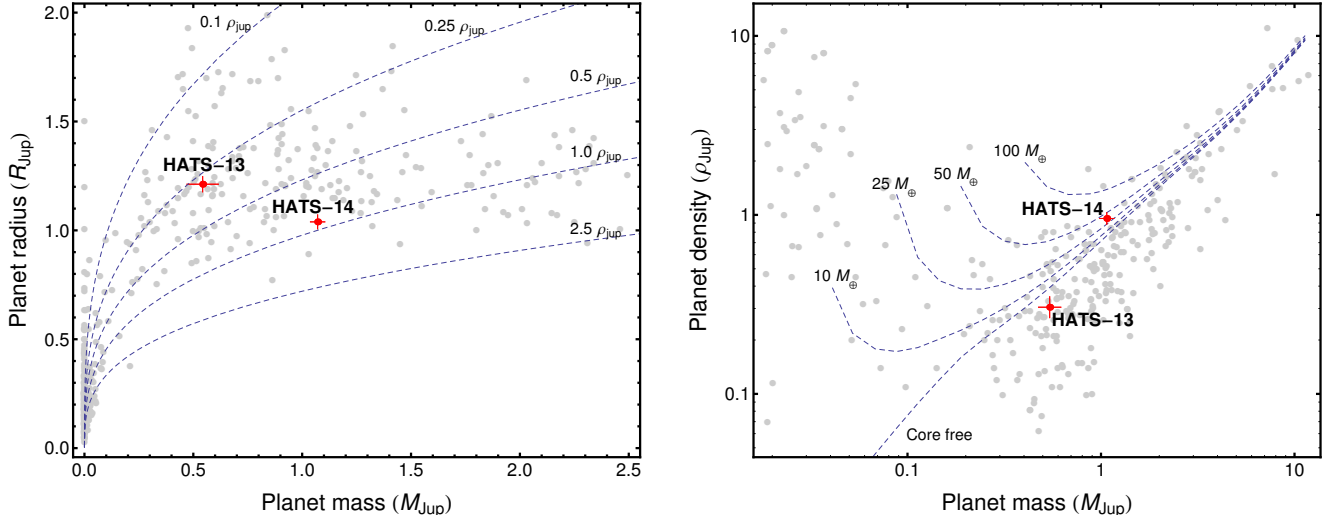


Fig. 6. *Left panel:* Masses and radii of the known transiting extrasolar planets. The grey points denote values taken from TEPCat. Their error bars have been suppressed for clarity. HATS-13b and HATS-14b are shown with red points with error bars. Dotted lines show where density is 2.5, 1.0, 0.5, 0.25 and 0.1 ρ_{J} . *Right panel:* the mass-density diagram of the currently known transiting exoplanets (taken from TEPCat). Again HATS-13b and HATS-14b are shown with red points with error bars. Four planetary models with various core masses (10, 25, 50 and 100 Earth mass) and another without a core (Fortney et al. 2007) are plotted for comparison.

0.5 M_{J} and inflated radii. In addition to the position of the planets, the right panel also shows 3.2 Gyr isochrones of giant planets at 0.045 au orbital separation from a solar analogue (Fortney et al. 2007). The plot suggests that HATS-13b should be a core-free planet, while HATS-14 should have a massive core of $\sim 50 M_{\oplus}$ (we stress that, although we cannot rule out the possibility that HATS-14 has a stellar companion which is diluting the transit – see discussion in Sect. 3.2 – our 3σ upper limit on the radius of the planet under this scenario is 1.11 R_{J}).

Acknowledgements. Development of the HATSouth project was funded by NSF MRI grant NSF/AST-0723074, operations have been supported by NASA grants NNX09AB29G and NNX12AH91H, and follow-up observations receive partial support from grant NSF/AST-1108686. A.J. acknowledges support from FONDECYT project 1130857, BASAL CATA PFB-06, and project IC120009 “Millennium Institute of Astrophysics (MAS)” of the Millennium Science Initiative, Chilean Ministry of Economy. R.B. and N.E. are supported by CONICYT- PCHA/Doctorado Nacional. R.B. and N.E. acknowledge additional support from project IC120009 “Millennium Institute of Astrophysics (MAS)” of the Millennium Science Initiative, Chilean Ministry of Economy. V.S. acknowledges support from BASAL CATA PFB-06. K.P. acknowledges support from NASA grant NNX13AQ62G. This work is based on observations made with telescopes at the ESO Observatory of La Silla. This paper also uses observations obtained with facilities of the Las Cumbres Observatory Global Telescope. Work at the Australian National University is supported by ARC Laureate Fellowship Grant FL0992131. We acknowledge the use of the AAVSO Photometric All-Sky Survey (APASS), funded by the Robert Martin Ayers Sciences Fund, and the SIMBAD database, operated at CDS, Strasbourg, France. Operations at the MPG 2.2m Telescope are jointly performed by the Max Planck Gesellschaft and the European Southern Observatory. The imaging system GROND has been built by the high-energy group of MPE in collaboration with the LSW Tautenburg and ESO. We thank Régis Lachaume for his technical assistance during the observations at the MPG 2.2m Telescope. We are grateful to P. Sackett for her help in the early phase of the HATSouth project. The reduced light curves presented in this work will be made available at the CDS (<http://cdsweb.u-strasbg.fr/>). We acknowledge the use of the following internet-based resources: the ESO Digitized Sky Survey; the TEPcat catalog; the SIMBAD data base operated at CDS,

Strasbourg, France; and the arXiv scientific paper preprint service operated by Cornell University.

References

- Alsubai, K. A., Parley, N. R., Bramich, D. M., et al. 2013, *AcA*, 63, 465
- Bakos, G. Á., Noyes, R. W., Kovács, G., et al. 2004, *PASP*, 116, 266
- Bakos, G. Á., Torres, G., Pál, A., et al. 2010, *ApJ*, 710, 1724
- Bakos, G. Á., Csubry, Z., Penev, K., et al. 2013, *PASP*, 125, 154
- Bayliss, D., Zhou, G., Penev, K., et al. 2013, *AJ*, 146, 113
- Brahm, R., Jordán, A., Hartman, J. D., et al. 2015, submitted to *AJ*, arXiv:1503.00062
- Charbonneau, D., Berta, Z. K., Irwin, J., et al. 2009, *Nature*, 462, 891
- Cardelli, J. A., Clayton, G. C., Mathis, J. S. 1989, *ApJ*, 345, 245
- Claret, A. 2004, *A&A*, 428, 1001
- Dopita, M., Hart, J., McGregor, P., et al. 2007, *Ap&SS*, 310, 255
- Dressing, C. D., Charbonneau, D. 2013, *ApJ*, 767, 95
- Fressin, F., Torres, G., Charbonneau, D., et al. 2013, *ApJ*, 766, 81
- Fortney, J. J., Marley, M. S., Barnes, J. W. 2007, *ApJ*, 659, 1661
- Fortney J. J., Lodders K., Marley M. S., Freedman R. S., 2008, *ApJ*, 678, 1419
- Fortney, J. J., Shabram, M., Showman, A. P., 2010, *ApJ*, 709, 1396
- Greiner, J., Bornemann, W., Clemens, C., et al. 2008, *PASP*, 120, 405
- Hansen, B. M. S., & Barman, T. 2007, *ApJ*, 671, 861
- Hartman, J. D. 2010, *ApJ*, 717, 138
- Hartman, J. D., Bakos, G. Á., Béky, B., et al. 2012, *AJ*, 144, 139
- Hartman, J. D., Bayliss, D., Brahm, R., et al. 2014, to appear in *AJ*, arXiv:1408.1758
- Jordán, A., Brahm, R., Bakos, G. Á., et al. 2014, *AJ*, 148, 29
- Kaufer, A., & Pasquini, L. 1998, *Proc. SPIE*, 3355, 844
- Knutson, H. A., Howard, A. W., Isaacson, H. 2010, *ApJ*, 720, 1569
- Kovács, G., Zucker, S., Mazeh, T. 2002, *A&A*, 391, 369
- Kovács, G., Bakos, G. Á., Noyes, R. W. 2005, *MNRAS*, 356, 557
- Madhusudhan N., 2012, *ApJ*, 758, 36
- Madhusudhan N., Knutson, H., Fortney, J. J., Barman, T. 2014, in *Protostars and Planets VI*, ed. H. Beuther, R. S. Klessen, C. P. Dullemond, & Th. Henning (University of Arizona Press), 739
- Mancini, L., Southworth, J., Ciceri, S., et al. 2014, *MNRAS*, 443, 2391
- Mandel, K., Agol, E. 2002, *ApJ*, 580, L171
- Mayor, M., Queloz, D. 1995, *Nature*, 378, 355
- Mohler-Fischer, M., Mancini, L., Hartman, J. D., et al. 2013, *A&A*, 558, A55
- Noguchi, K., Aoki, W., Kawanomoto, S., et al. 2002, *PASJ*, 54, 855

- Pál, A., Bakos, G. Á., Torres, G., et al. 2008, *ApJ*, 680, 1450
- Pecaut, M. J., Mamajek, E. E. 2013, *ApJS*, 208, 9
- Penev, K., Bakos, G. Á., Bayliss, D., et al. 2013, *AJ*, 145, 5
- Pepper, J., Pogge, R. W., DePoy, D. L., et al. 2007, *PASP*, 119, 923
- Queloz, D., Mayor, M., Udry, S., et al. 2001, *Msngr*, 105, 1
- Petigura, E. A., Howard, A. W., Marcy, G. W. 2013, *PNAS*, 110, 19273
- Pollacco, D. L., Skillen, I., Collier Cameron, A., et al. 2006, *PASP*, 118, 1407
- Pierini, D., Šuhada, R., Fassbender, R., et al., 2012, *A&A*, 540, A45
- Sato, B., Kambe, E., Takeda, Y., Izumiura, H., Ando, H. 2002, *PASJ*, 54, 873
- Sato, B., Hartman, J. D., Bakos, G. Á., et al. 2012, *PASJ*, 64, 97
- Schlaufman, K. C. 2010, *ApJ*, 719, 602
- Seager, S., Mallén-Ornelas, G. 2003, *ApJ*, 585, 1038
- Southworth J., Wheatley P. J., Sams G., 2007, *MNRAS*, 379, L11
- Southworth, J., Hinse, T. C., Jørgensen, U., et al. 2009, *MNRAS*, 396, 1023
- Sozzetti, A., Torres, G., Charbonneau, D., et al. 2007, *ApJ*, 664, 1190
- Sozzetti, A., Bernagozzi, A., Bertolini, E., et al. 2013, *EPJWC*, 47, 03006
- Southworth, J. 2011, *MNRAS*, 417, 2166
- Wakeford, H. R., & Sing, D. K. 2015, *A&A*, 573, A122
- Wheatley, P. J., Pollacco, D. L., Queloz, D., et al. 2013, *EPJWC*, 47, 13002
- Yi, S., Demarque, P., Kim, Y.-C., et al. 2001, *ApJS*, 136, 417
- Zacharias, N., Finch, C. T., Girard, T. M., et al. 2012, *VizieR Online Data Catalog*, 1322, 0
- Zhou, G., Bayliss, D., Penev, K., et al. 2014, *AJ*, 147, 144

Appendix A: Supplementary tables

Table A.1. Light curve data for HATS-13 and HATS-14

Object ^a	BJD ^b (2,400,000+)	Mag ^c	σ_{Mag}	Mag(orig) ^d	Filter	Instrument
HATS-13	55419.49174	−0.01156	0.00605	0.00000	<i>r</i>	HS
HATS-13	55434.71221	−0.00680	0.00753	0.00000	<i>r</i>	HS
HATS-13	55413.40415	0.00030	0.00605	0.00000	<i>r</i>	HS
HATS-13	55416.44831	0.00714	0.00620	0.00000	<i>r</i>	HS
HATS-13	55352.52327	0.01857	0.00631	0.00000	<i>r</i>	HS
HATS-13	55422.53650	−0.00515	0.00599	0.00000	<i>r</i>	HS
HATS-13	55355.56742	0.00957	0.00621	0.00000	<i>r</i>	HS
HATS-13	55291.64236	0.02224	0.00758	0.00000	<i>r</i>	HS
HATS-13	55373.83182	0.01939	0.00907	0.00000	<i>r</i>	HS
HATS-13	55361.65578	−0.00370	0.00583	0.00000	<i>r</i>	HS

Notes.

This table is available in a machine-readable form in the online journal. A portion is shown here for guidance regarding its form and content.

^a Either HATS-13, or HATS-14.

^b Barycentric Julian Date is computed directly from the UTC time without correction for leap seconds.

^c The out-of-transit level has been subtracted. For observations made with the HATSouth instruments (identified by “HS” in the “Instrument” column) these magnitudes have been corrected for trends using the EPD and TFA procedures applied *prior* to fitting the transit model. This procedure may lead to an artificial dilution in the transit depths. For HATS-13 the transit depth is 95% that of the true depth, with for HATS-14 it is 93% that of the true depth. For observations made with follow-up instruments (anything other than “HS” in the “Instrument” column), the magnitudes have been corrected for a quadratic trend in time fit simultaneously with the transit.

^d Raw magnitude values without correction for the quadratic trend in time. These are only reported for the follow-up observations.

Table A.2. Relative radial velocities and bisector spans for HATS-13

BJD (2,456,000+)	RV ^a (m s ⁻¹)	σ_{RV} ^b (m s ⁻¹)	BS (m s ⁻¹)	σ_{BS} (m s ⁻¹)	Phase	Instrument
53.29791	84.91	91.40	0.711	CYCLOPS
56.26837	-27.19	23.00	0.687	CYCLOPS
57.29641	-204.59	21.20	0.025	CYCLOPS
59.28565	362.01	48.90	0.678	CYCLOPS
77.83581	116.30	25.00	-4.0	13.0	0.772	FEROS
78.82092	-52.70	28.00	11.0	13.0	0.096	FEROS
79.84891	-43.70	24.00	16.0	12.0	0.434	FEROS
80.78831	225.02	35.00	-62.0	26.0	0.742	Coralie
81.83369	-75.98	38.00	60.0	26.0	0.086	Coralie
81.92743	-71.70	26.00	-2.0	13.0	0.117	FEROS
82.93245	93.0	32.0	0.447	Coralie
83.89769	51.30	25.00	2.0	13.0	0.764	FEROS
84.78165	-101.98	43.00	-170.0	29.0	0.054	Coralie
85.85427	-179.70	28.00	-28.0	14.0	0.407	FEROS
85.93485	-228.98	42.00	-76.0	29.0	0.433	Coralie
86.93769	-36.70	37.00	1.0	17.0	0.762	FEROS
88.85705	-251.70	32.00	-47.0	15.0	0.393	FEROS
114.66035	131.30	30.00	-620.0	14.0	0.870	FEROS
115.81404	-50.70	30.00	-116.0	14.0	0.249	FEROS
116.76798	114.30	24.00	-18.0	12.0	0.562	FEROS
118.62415	-42.70	28.00	3.0	13.0	0.172	FEROS
119.82198	39.30	37.00	-26.0	17.0	0.565	FEROS
126.87056	104.30	30.00	27.0	14.0	0.881	FEROS
144.82638	125.30	50.00	-21.0	22.0	0.779	FEROS
145.89316	-98.70	45.00	91.0	20.0	0.130	FEROS
146.66661	14.30	47.00	35.0	21.0	0.384	FEROS
161.61887	-71.98	41.00	-17.0	29.0	0.296	Coralie
161.70929	-121.70	32.00	9.0	15.0	0.326	FEROS
164.51993	-52.98	47.00	-44.0	29.0	0.249	Coralie
165.67277	82.30	24.00	23.0	12.0	0.628	FEROS
171.58342	54.30	23.00	-10.0	12.0	0.569	FEROS
189.95720	-22.0	15.8	0.605	HDS
189.97192	-0.3	15.3	0.610	HDS
190.93418	43.16	15.52	-33.5	28.3	0.928	HDS
190.94892	43.99	12.45	-31.0	28.4	0.932	HDS
190.96364	12.14	18.41	13.7	21.4	0.937	HDS
191.93411	-66.61	25.00	11.8	21.8	0.256	HDS
191.94884	-40.51	25.97	28.6	19.4	0.261	HDS
191.96356	-75.01	31.07	16.9	41.5	0.266	HDS
192.92689	17.12	17.65	-18.4	18.0	0.582	HDS
192.93930	19.11	16.36	10.1	15.4	0.586	HDS
192.95172	52.12	17.50	24.2	22.9	0.590	HDS
192.96412	48.76	23.21	0.593	HDS
208.70072	109.30	37.00	-8.0	17.0	0.763	FEROS
209.62306	-77.70	37.00	-69.0	17.0	0.066	FEROS
215.61886	-28.70	33.00	78.0	15.0	0.035	FEROS
239.57386	137.02	43.00	63.0	26.0	0.905	Coralie
240.56437	-120.0	37.0	0.230	Coralie

Notes. Note that for the iodine-free template exposures we do not measure the RV but do measure the BS. Such template exposures can be distinguished by the missing RV value. The Subaru/HDS observation of HATS-13 without a BS measurement has too low S/N in the I₂-free blue spectral region to pass our quality threshold for calculating accurate BS values. We also exclude from the table one I₂-free Subaru/HDS observation of HATS-13 which had too low S/N to provide an accurate BS measurement.

^a The zero-point of these velocities is arbitrary. An overall offset γ_{rel} fitted independently to the velocities from each instrument has been subtracted.

^b Internal errors excluding the component of astrophysical jitter considered in Sect. 3.3.

Table A.3. Relative radial velocities and bisector spans for HATS-14

BJD (2,456,000+)	RV ^a (m s ⁻¹)	σ_{RV} ^b (m s ⁻¹)	BS (m s ⁻¹)	σ_{BS} (m s ⁻¹)	Phase	Instrument
77.90592	-89.89	27.00	-23.0	13.0	0.417	FEROS
78.86766	168.11	24.00	15.0	12.0	0.764	FEROS
114.77348	171.11	44.00	5.0	19.0	0.742	FEROS
114.85948	151.11	27.00	5.0	13.0	0.773	FEROS
116.65611	-69.89	26.00	36.0	13.0	0.422	FEROS
117.60502	140.11	37.00	41.0	17.0	0.765	FEROS
121.81588	-137.89	37.00	-13.0	17.0	0.287	FEROS
125.91876	142.11	33.00	14.0	15.0	0.770	FEROS
145.75487	47.11	37.00	-10.0	17.0	0.940	FEROS
160.71709	-147.10	39.00	-6.0	29.0	0.347	Coralie
161.81222	95.90	96.00	-19.0	37.0	0.743	Coralie
164.54335	190.90	43.00	140.0	29.0	0.730	Coralie
424.76755	162.11	33.00	12.0	15.0	0.784	FEROS
492.58995	-151.89	37.00	46.0	17.0	0.297	FEROS
618.55621	127.90	44.00	-53.0	32.0	0.826	Coralie
619.56771	-128.10	68.00	0.191	Coralie
620.56070	81.90	70.00	68.0	37.0	0.550	Coralie

Notes. As in Table A.2